Chem. **1986**, *24*, 748.
15. Harris, R. K.; Jones, J.; Ng, S. *J. Magn. Reson.* **1978**, *30*, 521.
16. Iwamiya, J. H.; Maciel, G. E. *J. Am. Chem. Soc.* **1993**, *115*, 6835.
17. Fukui, H. *Magn. Res. Rev.* **1987**, *11*, 205.
18. Chesnut, D. B. In *Annual Reports on NMR Spectroscopy*; Webb, G. A., Ed; Academic Press: New York, 1989; Vol. 21.
19. Pestunovich, V. A.; Shterenberg, B. Z.; Lippmaa, E. T.; Myagi, M. Ya.; Alla, M. A.; Tandura, S. N.; Baryshok, V. P.; Petukhov, L. P.; Voronkov, M. G. *Dokl. Akad. Nauk SSSR* **1981**, *258*, 1410.
20. (a) Csonka, G. I.; Hencsei, P. *J. Comput. Chem.* **1994**, *15*, 385. (b) Csonka, G. I.; Hencsei, P. *J. Comput. Chem.* **1996**, *17*, 767.
21. (a)Gauss, J. *J. Chem. Phys.* **1993**, *99*, 3629. (b) Olah, G. A.; Rasul, G.; Heiliger, L.; Prakash; G. K. S. *J. Am. Chem. Soc.* **1996**, *118*, 3580.
22. (a) Rauhut, G.; Puyear, K. W.; Pulay, P. *J. Phys. Chem.* **1996**, *100*, 6310. (b) Schreckenbach, G.; Ziegler, T. *J. Phys. Chem.* **1995**, *99*, 606.

Reaction of Gas-Phase Atomic Hydrogen with Chemisorbed Hydrogen Atoms on an Iron Surface

M. S. Kim and J. Ree*

Department of Chemistry, Chonnam National University
**Department of Chemistry Education, College of Education, Chonnam National University, Kwangju 500-757 Korea*
Received May 22, 1997

The reaction of gas-phase atomic hydrogen with hydrogen atoms chemisorbed on Fe(110) surface is studied by use of classical trajectory procedures. Flow of energy between the reaction zone and bulk solid phase has been treated in the generalized Langevin equation approach. A London-Eyring-Polanyi-Sato energy surface is used for the reaction zone interaction. Most reactive events are found to occur in strong single-impact collisions on a subpicosecond scale via the Eley-Rideal mechanism. The extent of reaction is large and a major fraction of the available energy goes into the vibrational excitation of H_2, exhibiting a vibrational population inversion. Dissipation of reaction energy to the heat bath can be adequately described using a seven-atom chain with the chain end bound to the rest of solid. The extent of reaction is not sensitive to the variation of surface temperature in the range of T_s=0-300 K in the fixed gas temperature, but it shows a minimum near 1000 K over the T_g=300-2500 K.

Introduction

An understanding of energy transfer among various modes in the interaction system on the surface is a prerequisite for a detailed appreciation of reactive events that follow. Many studies have thus addressed the dynamics of trapping and energy transfer on the surface and the subsequent desorption of the product molecule in gas-surface reactions.[1-3] Among others, it may be of special interesting to observe direct reactive interactions of gas-phase reactants with atoms or molecules chemisorbed on a metal surface to form a molecule that immediately desorbs from the surface. This so called the Eley-Rideal (ER) mechanism is less common than the Langmuir-Hinshelwood (LH) mechanism in which both reactants are adsorbed and in thermally equilibrium with the surface before the reaction occurs.[1,4] In the ER mechanism, the difference between the exothermicity of the gas-phase reaction and the heat of chemisorption is large. Thus elucidating the dynamics of intramolecular energy flow in the trapped state formed from an active gas-phase reactant containing excess energy and the distribution of the excess energy among various motions of the product has been an important problem in gas-surface reactions.[4-22]

Since chemisorption energies for H on a metal surface lie in the range of 2-3 eV,[23,24] the H-metal surface is an attractive reactive site to produce highly-excited products when the gas reactant to H attraction greatly exceeds this range. Rettner *et al.*[12,13] studied the reaction of gas phase H (D) with D(H) adsorbed on Cu(111). They showed the translational and internal energy and angular distribution of the HD product representing their sensitivity to the incident energy as well as to which isotope was incident. The spread of the translational energy distribution was found to range from zero to about the maximum available energy that is released in the ER mechanism for this system. Gates and coworkers have examined the reaction between gas phase H (D) and D(H) adsorbed on Si(100) and Si(111), and have suggested the ER mechanism based on kinetics studies and measured activation energies.[14,15] Kratzer and Brenig[16] performed 2D quantum mechanical calculations for the ER reaction of H atoms incident on H chemisorbed to W. They found that the H_2 product is formed in high vibrational

*To whom correspondence should be addressed

states. Jackson and Persson[17-20] have accomplished similar calculations for the ER formation of H_2 using potentials chosen to model reaction with H chemisorbed to W and Cu. They have also obtained a high degree of vibrational excitation, and they featured an important differences between the possible isotopic combinations of H and D. Shin[21] has explored the vibrational excitation of H_2 produced in the reaction between gas-phase and chemisorbed H atoms on a tungsten surface by use of classical trajectory procedures. He found that the precursor $H_{gas}\cdots H_{ads}$ is formed in the early stage of collision, retaining most of the initial excitation when it desorbs as H_2. We[22] also carried out classical trajectory calculations for the reaction of gas phase atomic O with H atoms chemisorbed on a corrugated tungsten surface, and observed that most reactive events occur in single-impact collisions on subpicosecond scale *via* the ER mechanism producing highly-excited OH.

The purpose of this paper is to study the reaction of gas-phase hydrogen atoms with hydrogen atoms chemisorbed on the Fe(110) surface. To our knowledge, this reaction has not been studied experimentally. Because the H-metal chemisorption energy and the stretching frequency are similar as Cu, this reaction is considered to show similar properties as Cu. In the H_{gas}+H_{ads}/Fe(110) system, the exothermicity of the gas-phase reaction $H+H\rightarrow H_2$ is large (= 4.478 eV), so that $\Delta E=E+D_{HH}-D_{HFe}=(E+2.07)$ eV is liberated after dissociating the H_{ads}-Fe bond in the case of on-top site on Fe(110). Here, E is the collision energy of H_{gas}, and D_{HH} and D_{HFe} are the dissociation energies of the H-H and H_{ads}-Fe bond, respectively. If there is a preferential build-up of energy in the H_2 vibration, the product can exhibit a population inversion. Therefore, the extent of reaction, extent of H_2 excitation, and energy dissipation in the solid should be determined in this gas-surface reaction. We formulate a London-Eyring-Polanyi-Sato (LEPS) potential energy surface for the H_{gas}-H_{ads}, H_{ads}-Fe, and H_{gas}-surface interactions in the reaction zone. We also employ the molecular time scale generalized Langevin formalism[25-27] to introduce a mechanism of energy transfer between the reaction zone and the bulk phase. On the other hand, Jackson and Persson have explored the similar quantum mechanical calculations for Cu and W using a flat surface model which neglects the dissipation of energy into the solid.[17-20] Thus, it should be interesting to compare our results with their calculations. At first, we are mainly concerned with the reaction taking place at the gas temperature (T_g) at 2500 K and the surface temperature (T_s) at 0 K, and then have extended to consider the dependence of reaction probabilities on both T_g and T_s.

Model and Numerical Procedures

We show the collision model for the reaction of the gas-phase H atom with the chemisorbed H atom on the iron atom chain in Figure 1. The gas atom interacts with the adatom (H_{ads}) and surface(S), characterized by chemisorption and physisorption types, respectively.[28] The pertinent coordinates are R and θ for H_{gas} and z_{HFe} for H_{ads}, determining the $H_{gas}\cdots H_{ads}$ distance $z_{HH}=(R-z_{HFe})/\cos\theta$, and the chain atom coordinates ξ's; see Figure 1. The $H_{ads}\cdots Fe_0$ interaction potential is assumed to depend on the coordinates

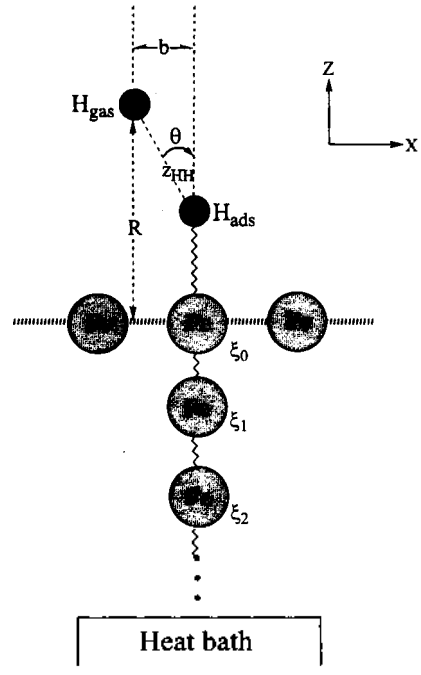

Figure 1. Collision coordinates. The gas atom approaches the surface and the H atom chemisorbed to the Fe_0 atom are shown. The chain atoms bound to the center atom (0) are numbered 1, 2, ..., N, with the vibrational coordinates ξ_0, ξ_1, ξ_2,....., ξ_N.

of the $H_{ads}-Fe_0$ bond, $z_{HFe}=d_{HFe}+x$, and the surface atom 0, ξ_0. Here, d_{HFe} and x are the equilibrium bond distance and displacement of the H-Fe_0 bond, respectively. We consider a chain of Fe atoms which couples the reaction zone to the bulk phase. The chain atoms are numbered n=0, 1, 2, ..., N; see Figure 1. The motions of the chain is considered to provide a simple quasiphysical picture of energy flow between the reaction zone and the heat bath. All these (N+1)-chain atoms interact directly with the gas atom. We thus consider the reaction zone atoms (H_{gas}, H_{ads}, Fe_0) and N chain atoms belonging to the *primary* system and solve the equations of motion for an appropriately chosen potential energy surface. We denote the remaining infinite number of solid atoms as *secondary* atoms. The secondary atoms influence the dynamics of the primary system through dissipative and stochastic force terms, which explicitly enter in the Nth equation of motion. These two terms balance, according to the fluctuation-dissipation theorem, so that the proper temperature is maintained in the primary zone.[25,27] In this model of over-simplication of the solid structure, we have ignored some possibly important factors, such as the nearest neighbor site interactions along the chain and the crystallographic orientation. But, we showed that the energy flow along the collinear configuration is the most important in the gas-surface interaction, and the inclusion of additional solid atom chains to the model does not significantly affect the outcome of reactive events.[29] Kubiak *et al.* reported also that the Cu(110) data are identical to the Cu(111) data to within the experimental accuracy in the dynamics study of H_2 and D_2 recombinatively desorbing from Cu(110) and Cu(111) surfaces.[30] Thus, we replace the bulk solid phase by a single fictitious N-atom-composed nearest neighbor harmonic chain which is bound to the rest of solid.

Table 1. Interaction parameters

Interaction	$H_{gas}\cdots H_{ads}$	$H_{ads}\cdots Fe_0$	$H_{gas}\cdots S$
D (eV)†	4.478(32)#	2.409(33)	0.038**
ω (cm^{-1})	4401(32)	1280(33)	
R_e (Å)	0.741(32)	1.36(33)	3.0(34)**
a (Å)	0.257*	0.445*	0.40**
	$\Theta_D=\hbar\omega_D/k=467$ K## (35)		

†$D=D_0+\frac{1}{2}\hbar\omega$, where D_0 is taken from the reference. #Parentheses include references. *Calculated from $a=(D/2m)^{1/2}\omega$. **See text. ##The Debye temperature is needed in using ω_{en}, ω_{cn}, Ω_n, and β_n.

The incident atom with the collision energy E becomes trapped at the adatom site. The trapped atom undergoes a strong interaction with H_{ads} on the surface, causing energy flow from the $H_{gas}\cdots H_{ads}$ vibration to the $H_{ads}\cdots Fe_0$ bond in the complex $H_{gas}\cdots H_{ads}\cdots Fe_0$. When the $H_{ads}\cdots Fe_0$ bond weakens after gaining sufficient energy, H_2 can desorb after a residence time. Otherwise, H will rebound into the gas phase without reaction. The H_{gas}-surface distance z_{HS} is the relative coordinate R and the $H_{gas}\cdots H_{ads}$ distance is $z_{HH}=(R-z_{HFe})/\cos\theta$. We describe each atom-atom interaction energy in the reaction region by an exponential function containing both repulsive and attractive terms and model the interaction in the form of the London-Eyring-Polanyi-Sato (LEPS) type[30,31] as

$$U=\frac{1}{1+\Delta}\{V_{HH}+V_{HFe}+V_{HS}-[A_{HH}^2+A_{HFe}^2+A_{HS}^2 -A_{HH}A_{HFe}-(A_{HH}+A_{HFe})A_{HS}]^{1/2}\}, \quad (1)$$

where

$$V_i=\frac{1}{4}D_i\{(3+\Delta)\exp[(z_{ie}-z_i)/a_i]-(2+6\Delta)\exp[(z_{ie}-z_i)/2a_i]\}$$

and

$$A_i=\frac{1}{4}D_i\{(1+3\Delta)\exp[(z_{ie}-z_i)/a_i]-(6+2\Delta)\exp[(z_{ie}-z_i)/2a_i]\}$$

for i=HH, HFe, and HS. Here, z_{ie} is the equilibrium value of the distance z_i and Δ is an adjustable Sato parameter. The potential parameters are listed in Table 1.[32-35] Although there have been no data available on the physisorption of H atoms on a Fe surface, the information for the related system of H_2/Cu is known. For the latter, the well depth is 45 meV.[36] Assuming the ratio $D_{diatom,surface}/D_{atom,surface}=1.2$ to hold in this case,[37] we estimate $D_{HS}=0.038$ eV and take $a_{HFe}=0.4$ Å to reflect the characteristics of physisorption. The van der Waals radii of H and Fe are 120-145 pm and ~160 pm, respectively,[34] so we take $R_e=3$ Å. The explicit forms of V_i and A_i given above are now dependent on R, x, θ, and ξ_0; *i. e.*, the LEPS potential energy has the functional dependence on $U(R, x, \theta, \xi_0)$.

The value of the Sato parameter often lies in the range of −0.5 to 0.6 for atom-atom or atom-diatom reactions taking place for both the gas-surface system and the gas phase.[19,22,38-42] We adjust Δ such that the resulting potential minimizes the contribution of activation energy barrier and attractive potential well in the exit channel. The result is Δ=0.33. Figures 2(a, b) show the potential energy surfaces calculated with this Sato parameter in the direction of θ=0° and 80°, respectively. The former exhibits a smooth entrance channel, whereas the latter shows the occurrence of a barrier in the entrance channel which is not shown explicitly. From finer calculations, the barrier is found to appear at the H-H distance of 2.29 Å and H-Fe distance of 1.52 Å. In the latter case, even though the barrier is low, the extent of reactive collision is significantly decreased, which will be discussed later.

In the present system, the dynamics of the H_{gas}+H_{ads}-Fe_0 interaction is influenced by the inner Fe atoms. We assume these atoms, as well as 0 atom, to undergo harmonic vibration $V(\xi_n)=\frac{1}{2}M\omega_{en}^2\xi_n^2$, where M is the mass of Fe and ω_{en} is the Einstein frequency. Because of the cross terms, the sum of solid interaction potential energies includes terms such as $\frac{1}{2}M\omega_{cn}^2\xi_{n-1}\xi_n$, $\frac{1}{2}M\omega_{c,n+1}^2\xi_n\xi_{n+1}$, etc., where ω_{cn} is the coupling constant characterizing the chain. Thus, with the LEPS function given above, we can express the overall interaction potential for the present system in the

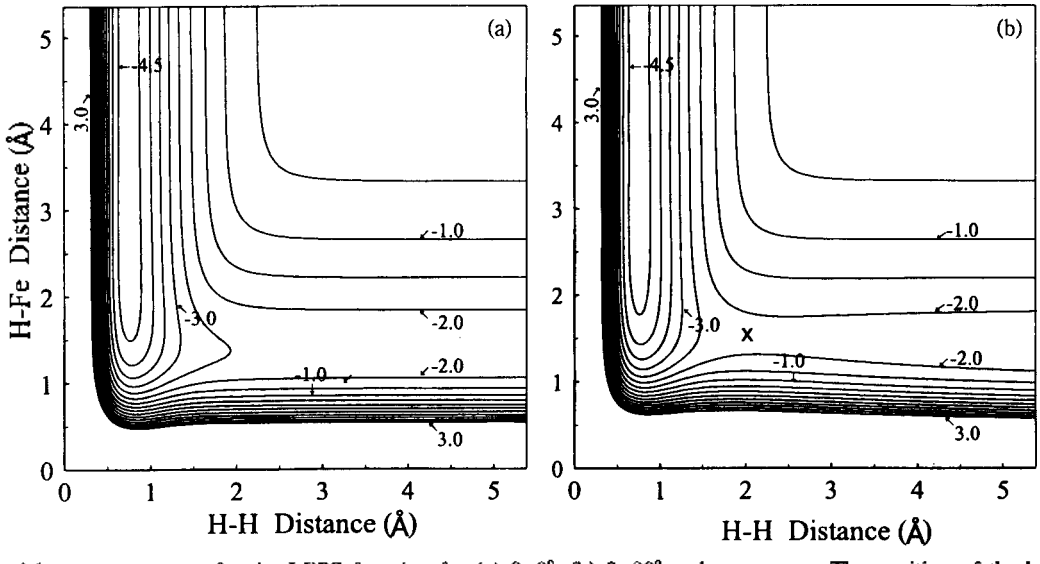

Figure 2. Potential energy contours for the LEPS function for (a) θ=0°. (b) θ=80° and $z_{HFe_0}=z_{HFe_0,e}$. The position of the barrier is indicated by a cross. The labeled contours are in eV.

form

$$U(R,x,\theta,\{\xi_i\})=\frac{1}{1+\Delta}\{V_{HH}+V_{HFe}+V_{HS} -[A_{HH}^2+A_{HFe}^2+A_{HS}^2-A_{HH}A_{HFe}-(A_{HH}+A_{HFe})A_{HS}]^{1/2}\} +\sum_i(\tfrac{1}{2}M\omega_{ci}^2\xi_i^2)+\sum_i(\tfrac{1}{2}M\omega_{ci}^2\xi_{i-1}\xi_i,\ \tfrac{1}{2}M\omega_{c,i+1}^2\xi_i\xi_{i+1},\ \text{etc.}), \tag{2}$$

where the notation $\{\xi_i\}$ denotes the set of chain atom coordinates (ξ_0, ξ_1, ξ_2, ... ξ_n).

The gas-phase H atom approaches the surface at the impact parameter b. In the initial approach, the angle between the $H_{gas}\cdots H_{ads}$ axis and the surface normal is represented by $\theta=\tan^{-1}[b/(R-z_{HFe})]$. When the $H_{gas}\cdots H_{ads}$ interaction sets in, however, θ varies according to the angular velocity equation $d\theta(t)/dt=(2E/\mu)^{1/2}\,b/Z_{HH}^2$, where μ is the reduced mass associated with the H···surface interaction. A united set of the effective equations of motion for the reaction zone and N chain atoms can then be written as

$$\mu\ddot{R}(t)=-\partial U(R,x,\theta,\{\xi_i\})/\partial R, \tag{3a}$$

$$\mu_{HFe}\ddot{x}(t)=-\partial U(R,x,\theta,\{\xi_i\})/\partial x, \tag{3b}$$

$$\dot{\theta}(t)=(2E/\mu)^{1/2}\,b/z_{HH}^2, \tag{3c}$$

$$M\ddot{\xi}_0(t)=-M\omega_{c0}^2\xi_0(t)+M\omega_{c1}^2\xi_1(t)-\partial U(R,x,\theta,\{\xi_i\})/\partial\xi_0, \tag{3d}$$

$$M\ddot{\xi}_1(t)=-M\omega_{c1}^2\xi_1(t)+M\omega_{c1}^2\xi_0(t)+M\omega_{c2}^2\xi_2(t), \tag{3e}$$

$$M\ddot{\xi}_2(t)=-M\omega_{c2}^2\xi_2(t)+M\omega_{c2}^2\xi_1(t)+M\omega_{c3}^2\xi_3(t), \tag{3f}$$

$$\cdots\cdots\cdots\cdots\cdots\cdots\cdots\cdots\cdots\cdots\cdots\cdots\cdots\cdots$$

$$M\ddot{\xi}_{N-1}(t)=-M\omega_{c,N-1}^2\xi_{N-1}(t)+M\omega_{c,N-1}^2\xi_{N-2}(t)+M\omega_{cN}^2\xi_N(t), \tag{3g}$$

$$M\ddot{\xi}_N(t)=-M\Omega_N^2\xi_N(t)+M\omega_{cN}^2\xi_{N-1}(t)-M\beta_{N+1}\dot{\xi}_N(t)+Mf_{N+1}(t). \tag{3h}$$

Here μ_{HFe} is the reduced mass associated with the H-Fe_0 bond. The $H_{gas}\cdots H_{ads}$ interaction dominates others in the LEPS potential, so that the HH force term in the r.h. side of Eq. (3a) is of major importance in determining the collision trajectory R. Eq. (3c) determines the variation of θ during the interaction for a given value of b. Eqs. (3d-h) for n=0, 1, 2, ..., N are the chain representation of the many-body dynamics and correctly describe the short-time (Einstein limit) processes. In Eqs. (3d-h), ω_{cn} and ω_{cn} are the short-time scale effective harmonic frequencies and Ω_N is the adiabatic frequency. At short time the nth oscillator responds like an isolated harmonic oscillator with frequency ω_{cN}, whereas Ω_N determines the long-time response of the heat bath. The friction coefficient β_{N+1} governs the dissipation of energy to the heat bath, which occurs long after the reaction.[29] The quantity $Mf_{N+1}(t)$ in the Nth equation is governed by the fluctuation-dissipation theorem $\langle f_{N+1}(t)\cdot f_{N+1}(0)\rangle=(6kT_s/M)\beta_{N+1}(t)$.[27] The values of ω_{cN}, ω_{cn}, Ω_N, and β_N are given elsewhere[29]; the Debye temperature $\Theta_D=\hbar\omega_D/k$=467 K.[35] With computationally convenient friction kernels and fluctuating forces, Eqs. (3a-h) offer an approximate but realistic way of handling many-body coupling of the reactants to the solid atoms in the primary zone and then the primary zone to the heat bath.

Results and Discussion

Computational Details. The computational routines include Monte Carlo procedures[43] to generate random numbers. We first sample collision energies E at T_g in accordance with the Maxwell distribution function $f(E, T_g) \propto e^{-E/kT_g}$. This sampling is important in studying the temperature dependence, since each atom with a given collision energy collides with the surface and undergoes reaction. In sampling impact parameters b, we note that $d_{Fe\text{-}Fe}$ is 2.52 Å,[44] whereas $z_{HH,e}$ is 0.741 Å,[32] so that $1.7z_{HH,e}$ is very close to the half-way point between two adjacent surface atoms. (Hereafter, we express $z_{HH,e}$ by z_e). Thus, we only consider gas atoms approaching the surface with an impact parameter in the range $0\le b/z_e<1.7$. The initial condition for solving Eq. (3c) is $\theta(t_0)=\tan^{-1}\{b/[R(t_0)-z_{HFe}(t_0)\}$, where $R(t_0)=R_e+a\ln[(D/E)+(D/E)^2]+2a\ln\{\cosh[(E/2\mu)^{1/2}(t_0/a)]-[D/(E+D)]^{1/2}\}$, and $z_{HFe}(t_0, E_{v,HFe}^0, \delta_{HFe})=z_{HFe,0}+2a_{HFe}\ln\{[1+(E_{v,HFe}^0/D_{HFe})]^{1/2}\sin(\Lambda_{HFe}t_0+\delta_{HFe})\}/[1-(E_{v,HFe}^0/D_{HFe})]\}$. Here, $\Lambda_{HFe}=[2(D_{HFe}-E_{v,HFe}^0)/\mu_{HFe}]^{1/2}/2a_{HFe}$, D and a are the potential constants for the $H_{gas}\cdots H_{ads}$ interaction, and D_{HFe}, a_{HFe}, δ_{HFe} and $E_{v,HFe}^0$ are the potential constants, initial phase and vibrational energy of the H-Fe_0 bond, respectively. We also consider the H-Fe_0 vibration to be initially in accordance with the Maxwell distribution function $g(E_{v,HFe}^0, T_s) \propto e^{-E_{v,HFe}^0/kT_s}$. Therefore, we need to sample E, $E_{v,HFe}^0$, δ_{HFe}, and b. For the nth chain atom, the initial conditions are $\xi_n(t_0)=A_n\sin(\omega_{cn}t_0+\delta_n)$ and $\dot{\xi}_n(t_0)=\omega_{cn}[A_n^2-\xi_n^2(t_0)]^{1/2}$, where $A_n^2=2kT/M\omega_{cn}^2$ and the phase δ_n is randomly sampled. Once the initial conditions are sampled, Eqs. (3a-h) can be solved by standard trajectory methodology.[21,43,45] In solving these equations, we began trajectories at a distance $R(t_0)$ or 15 Å, and the equations are integrated until trajectories proceed to at least 50 Å from the surface after the final turning point. We define the reaction time t_R as the time at which the center of $H_{gas}\cdots H_{ads}$ bond reaches 5 Å after passing through the final turning point. The time step in the integration is set at 0.25 f_s or 1/30th the vibrational period of H_2, the shortest period in the reaction system.

We first consider the effect of chain length on the reaction to establish the optimum size of the chain for a realistic calculation of reactive events. For this purpose, we take some representative trajectories of single-turning-point (STP) reactive event and compute the dependence of energy transfer to the solid E_s on N at T_g=2500 K and T_s=0 K. In these calculations, Eq. (3h) is replaced by $M\dot{\xi}_N(t)=-M\omega_{cN}^2\xi_N(t)+M\omega_{cN}^2\xi_{N-1}(t)$ to neglect the dissipative mechanism. When there is no dissipative mechanism, the energy transferred to the $(N+1)$ chain $E_s(t)$ remains without dissipation into the inner region of the solid, so that the limiting value $E_s(\infty)$ is constant. As N increases, the limiting value $E_s(\infty)$ oscillates, leveling off to the constant value after N=6. This indicates that we can do a realistic calculation of the gas-surface reaction with a relatively small number of heat bath atoms. Throughout this work, we will therefore use the 7-atom chain (*i.e.*, N=6).

Distribution of Collision Times. The interaction begins at near t=0, and then the incident atoms either rebound to the gas phase or combine with the adatom to form a H_2 molecule. Of 10000 trajectories sampled in $0\le b/z_e<1.7$, 1736 have produced H_2. These trajectories are distributed over a range of reaction times t_R; this distribution is shown in Figure 3. These reactive trajectories have their reaction times in the range of 0 to 3.5 ps. Moreover, 1391 of 1736

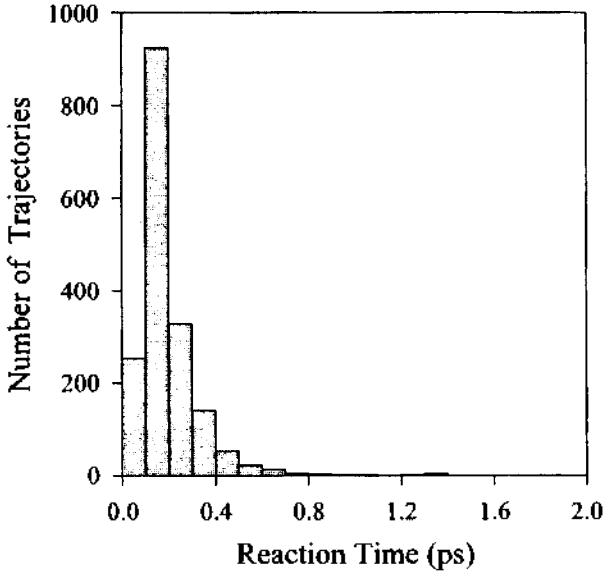

Figure 3. Distribution of reaction times.

trajectories undergo STP collisions on a subpicosecond scale ($t_R \leq 0.5$ ps). Peden and co-workers have considered the reaction to follow the ER mechanism, if its reaction time is less than 10 ps.[46] If we apply the latter time scale, essentially all reactive events clearly follow the ER mechanism.

Dynamics of Reactive Collisions. To examine details of the time evolution, we selected a trajectory which is representative of the single-impact collision at T_g=2500 K and T_s=0 K, and plotted the evolution of pertinent quantities in Figure 4. In Figure 4a, we show the collision trajectory, $H_{gas}\cdots H_{ads}$ distance, and $H_{ads}\cdots Fe_0$ distance. The incident atom is trapped for a short time on the surface at the beginning of collision, forming a loosely bound state $H_{gas}\cdots H_{ads}$ in the upper region of the potential well, and exchanges energy with the H_{ads}-Fe_0 bond. H_2(g) will form when the amount of energy transfer to the H_{ads}-Fe_0 bond exceeds the dissociation threshold D_{HFe_0}. Otherwise, either the H_{gas} atom rebounds from the surface or it becomes trapped on the adatom site permanently, forming H_2 in the adsorbed state. For the present system, however, the latter fraction is negligible. In this figure, we also show that the vibration of $H_{gas}\cdots H_{ads}$ is in near resonance with the $H_{ads}\cdots Fe_0$ vibration in a complex $H_{gas}\cdots H_{ads}\cdots Fe_0$. In fact, a near-resonant variation of these bonds is also seen in the time evolution of $E_{v,H_2}(t)$ and $E_{v,HFe}(t)$; Figure 4b. Here, we can determine the time dependence of the vibrational energy of $H_{gas}\cdots H_{ads}$ and $H_{ads}\cdots Fe_0$ bond in each collision from the expressions

$E_{v,H_2}(t)=\frac{1}{2}\,\mu_{H_2}\dot{z}_{HH}(t)^2+D\,[1-e^{-z_{HH}(t)/2a}]^2$ and

$E_{v,HFe_0}(t)=\frac{1}{2}\,\mu_{HFe}\,[\dot{z}_{HFe}(t)-\dot{\xi}_0(t)]^2+D_{HFe}\,\{1-e^{-[z_{HFe}(t)-\xi_0(0)]/2a_{HFe}}\}^2$,

respectively. The sharp variation of these energies during the impact indicates an efficient flow of energy from the newly formed $H_{gas}\cdots H_{ads}$ bond to $H_{ads}\cdots Fe_0$ in the complex $H_{gas}\cdots H_{ads}\cdots Fe_0$ on the surface as a result of a strong collision between the H_{gas} and H_{ads} atoms. The time evolution of $E_{v,H_2}(t)$ shown in Figure 4b indicates that the deactivation of high-energy $H_{gas}\cdots H_{ads}$ occurs in a single step losing a large amount of energy (>>kT), most of which transfers to $H_{ads}\cdots Fe_0$. The essential part of energy flow from $H_{gas}\cdots H_{ads}$

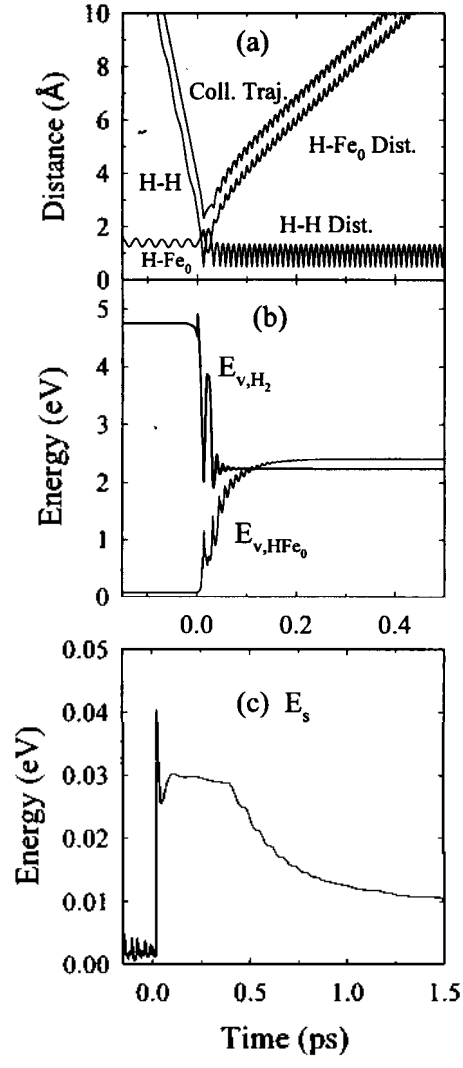

Figure 4. Time-evolution of the representative trajectory: (a) The collision trajectory, H-Fe_0 distance, and H_{gas}-H_{ads} distance, (b) the time evolution of the vibrational energies of H_2 and H-Fe_0, and (c) the solid energy with dissipation.

completed during the compression of $H_{gas}\cdots H_{ads}$ toward the closest approach in a short period of 0.1 ps. $H_{gas}\cdots H_{ads}$ stabilizes to H_2 as it stretches out from the closest approach and desorbs at $t\approx 0.2$ ps with $E_{v,H_2}(t)$=2.237 eV. That is, molecule H_2 desorbs with significant vibrational excitation, accompanied by some translational energy. Figure 4c shows the energy buildup in the solid chain on the $H_{gas}\cdots H_{ads}$ impact and its slow dissipation into the heat bath. In this figure, the dissipation process is shown up to t=1.5 ps, but even at several picoseconds after reaction, the dissipation is still in progress. The $H_{gas}\cdots H_{ads}$ attractive energy at the beginning of collision is 4.751 eV, and after dissociating the H_{ads}-Fe_0 bond, the remaining energy and the collision energy for the representative trajectory considered in Figure 4 are distributed among various motions of the product H_2 as E_{v,H_2}=2.237 eV, E_{r,H_2}=0.503 eV, E_{t,H_2}=0.0314 eV, and E_s= 0.0299 eV. That is, nearly all the energy liberated in the reaction is carried by the gas phase H_2.

The ensemble average of selected effects of all STP collisions should provide a great insight into the dynamic as-

pect of the reaction. Figure 5b shows the ensemble averaged time evolution of the vibrational energy of H_2, $E_{v,H_2}(t)$, in these STP collisions. Comparing this curve with the collision trajectory shown in Figure 5a, the incident atom resides at the surface for a short period of about 0.3 ps before desorbing as H_2. The vibrational energy curve begins with D_{H_2} at t_0 and rapidly decreases to the limiting value $E_{v,H_2}(\infty)$ =2.175 eV. Also shown in Figure 5b is the time evolution of the rotational energy, $E_{r,H_2}(t)$. It increases in the trapped state and then levels off to the limiting value 0.434 eV, which is much less than $E_{v,H_2}(\infty)$. The translational energy of the desorbing H_2 is 0.219 eV. In Figure 5c, we plot the time evolution of the ensemble averaged vibrational energy of the solid with or without the energy dissipative mechanism. In the non-dissipative case, the energy that has accumulated in the chain remains in it; *i.e.*, $E_s(t)$ levels off to a constant value of about 0.029 eV as $t\rightarrow\infty$; see the upper curve. On the other hand, in the presence of the dissipative mechanism, $E_s(t)$ slowly dissipates into the heat bath. Even at t=4.5 ps, about 14% of $E_s(t)$ has not yet dissipated. It takes many picoseconds to complete dissipation, representing that the many-body effect does not affect the short-time reactive event, in which the product has departed from the surface long before energy dissipation.

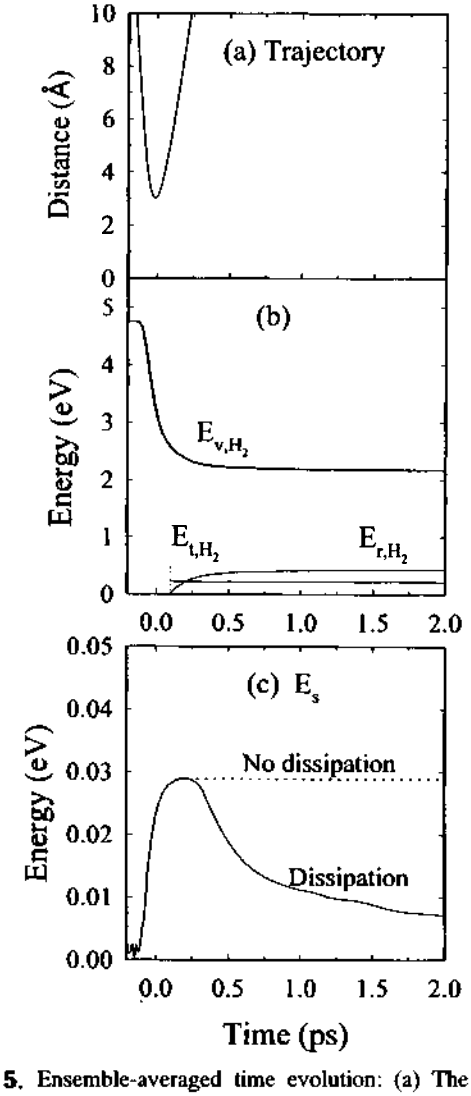

Figure 5. Ensemble-averaged time evolution: (a) The collision trajectory, (b) the vibrational and rotational energies of H_2, and (c) the solid energy with or without dissipative mechanism. In (b), the dotted line indicates the reaction threshold.

Energy Distribution and Reaction Probability. In Figure 6, we show the distribution of the vibrational, rotational, translational energies of H_2, and energies transferred to the solid in $0\leq b/z_e < 1.7$ for all reactive events at T_g=2500 K and T_s=0 K. Figure shows significant results on the dependence of these energies on the impact parameter. In Figure 6a, H_2 molecules produced in a small b collision are vibrationally highly excited and there are many such reactive events. The vibrational energy decreases with increasing b, but the number of reactive events is greatly diminished in such large-b collisions. The mean vibrational energy of the desorbed H_2 molecules is 2.145 eV. In Figure 6b, rotational excitation in small-b collisions is very small, but it is of significance in large-b collisions. However, the number of reactive events is very small when b is large, so that the problem of rotational excitation in the present gas-surface reaction is less important than the vibrational excitation. In Figure 6c, the translational energy of the reactive product H_2 molecule decreases with increasing b, but the rate of decrease is slower than the vibrational excitation. Particularly, these translational energies are lower than vibrational energies of H_2, in the range of 0.0005 to 1.323 eV. The mean translational energy of the desorbed H_2 molecules is 0.227 eV. Rettner[47] reported that the mean kinetic energy of the HD produced in the reaction of a beam of H(D) atoms with D(H) atoms chemisorbed on a Cu(111) surface at 100 K is close to 1 eV, independent of final angle within a range of $\pm 20^\circ$ of the surface normal. Jackson and Persson also reported that the average translational energy calculated at normal incidence with the incident energy E_i=0.075 eV for the reaction between a gas phase H atom and an adsorbed H atom is ~0.85 eV.[19] The latter values are significantly higher than the value calculated in the present system. In Figure 6d, energies transferred to the solid are remarkably small, in the range of 0.0002 to 0.118 eV. These also decrease with increasing b, and the mean energy is 0.03 eV. This value is significantly small compared to the mean calculated energy transferred to the solid in the reaction of gas-phase oxygen atoms with carbon monoxide molecules adsorbed on a platinum surface, 0.6 eV.[29]

In Figure 7a, we plot the reaction probability $P(b)=N_R(b)/N(b)$ as a function of b, where $N_R(b)$ and $N(b)$ are the reactive and total numbers of trajectories in a given b range, respectively. The probability takes a maximum value of 0.64 at $0\leq b<0.1$. Then, as b increases from zero, P(b) sharply decreases. As noted in Sec. 2, the incident atom approaches the surface with the H_{gas} to H_{ads} direction at the angle $\theta=\tan^{-1}[b/(R-z_{HFe})]$ from the surface normal. When the $H_{gas}\cdots H_{ads}$ interaction begins, however, θ varies according to the angular velocity equation $d\theta(t)/dt=(2E/\mu)^{1/2}b/z_{HH}^2$ until $t=t_{FTP}$ (*i.e.*, the time at the first turning point), where z_{HH} is dependent on the interaction potential. At the instant of the first impact, this equation gives the solution θ_{FTP}, which can be considered as the "true" incident angle toward to the adatom. For all reactive collisions, this angle varies approximately linearly with the impact parameter. The angles are confined to the angle of 0 to 60°. In a collision with $b>z_e$, most of

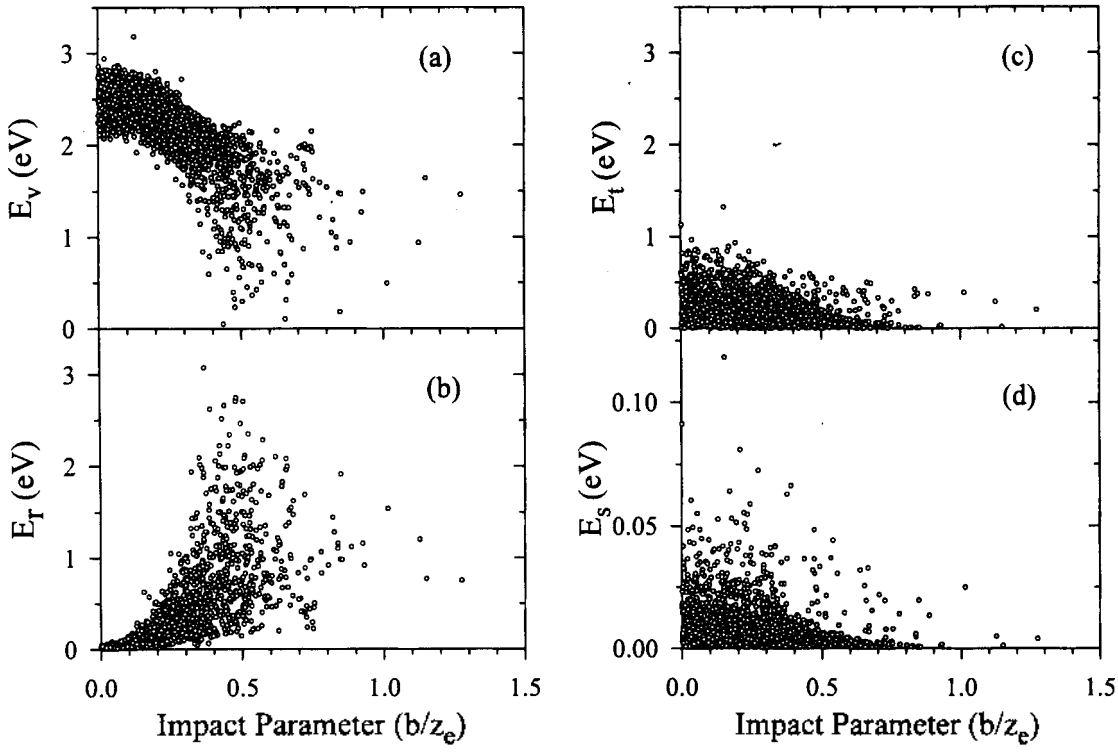

Figure 6. Dependence of (a) the vibrational energy, (b) the rotational energy, (c) the translational energy, and (d) the energy transferred to the solid on the reduced impact parameter b/z_e.

these angles are over 60°, and then the reaction probability is significantly small. The potential energy surface for over 60° is quite different with for 0°; see Figure 2b. For the former there is a barrier in the entrance channel. Moreover, if the angle of incidence of the H_{gas} with respect to the surface normal is over 60°, incident (normal) energy E is then less than one quarter of the total translational energy. Thus, the incident atom from $\theta_{FTP}>60°$ is less likely to overcome this barrier. Finally, H_2 formation ceases for $b/z_e>1.3$.

On the other hand, we can express the classical reaction cross section, corresponding to P(b) determined above in the form $\sigma=2\pi\int_0^\infty P(b)\,b\,db$. The result is $\sigma=0.268$ Å^2 at $T_g=2500$ K and $T_s=0$ K. It is interesting to compare the calculated cross section with $\sigma\approx0.5$ Å^2 for the H_2 formation on Cu(111) estimated in the collision energy range 0.05-0.25 eV by Persson and Jackson.[19] These calculated values are significantly smaller than the approximate values 4 ± 2.7 Å^2 and 5.4 ± 1.3 Å^2 which are estimated from the observed reaction probabilities between H(D) and saturated overlayers of D(H) on Cu.[12] The reason the calculated values are significantly smaller than the experimental values seems due to the hot atom mechanism neglected in the calculations.[48]

Both E_{v,H_2} and P(b) decrease with increasing b; see Figures 6a and 7a. That is, the production of a large number of H_2 with high vibrational excitation and a small number with low excitation creates conditions for a vibrational population inversion; see Figure 7b. Here we reversed the E_{v,H_2} axis from 3.0 eV to 0 eV to reflect the situation that small-b collisions produce highly-excited H_2, whereas large-b collisions produce unexcited H_2. The maximum population occurs at $E_{v,H_2}=2.3$ eV, which corresponds approximately to v=4. A similar vibrational population inversion has been found in OH produced from the recombination of gas-phase oxygen atoms and chemisorbed hydrogen atoms on a tungsten surface,[22] and in CO_2 produced from the reaction of oxygen atoms with chemisorbed CO on a platinum surface.[7,29] In Figure 7c, we show the rotational population. As mentioned above, rotational excitation in small-b collisions is very small, even though the number of reactive trajectories is large in this region. But, rotational excitation is significant when b is large, while the number of reactive events is very small when b is large. Thus, the maximum population occurs at $0\le E_{r,H_2}<0.2$ eV. This suggests that the rotational excitation is not important in the desorption process.

Temperature Dependence of Reaction Probability. We consider the dependence of the extent of reaction on both T_g and T_s. The results provide valuable information on the dependence of reaction probabilities on surface and gas temperatures. Nearly all the reactive events occur in a single-impact collision. Thus, a direct reaction is in favor at the high gas temperature but is weakly dependent on the surface temperature. In Figure 8a, we plotted the reaction probability over the $T_s=0$-300 K for the fixed value of $T_g=2500$ K. It is then a total reaction probability P(T) and is different from $P(b)=N_R(b)/N(b)$ presented above, which is the probability at given impact parameter. The figure shows that the P(T) decreases only slightly with T_s in the surface temperature range. This indicates that the reaction energy comes primarily from the incident atom, which is the essential feature of the ER mechanism.[49] Futhermore, the fraction of adatoms in the H_{ads}-Fe_0 vibrational energy state corresponding to the first excited state at $T_s=300$ K is less than 0.22%, thus it is not important to consider excited H_{ads}-Fe_0

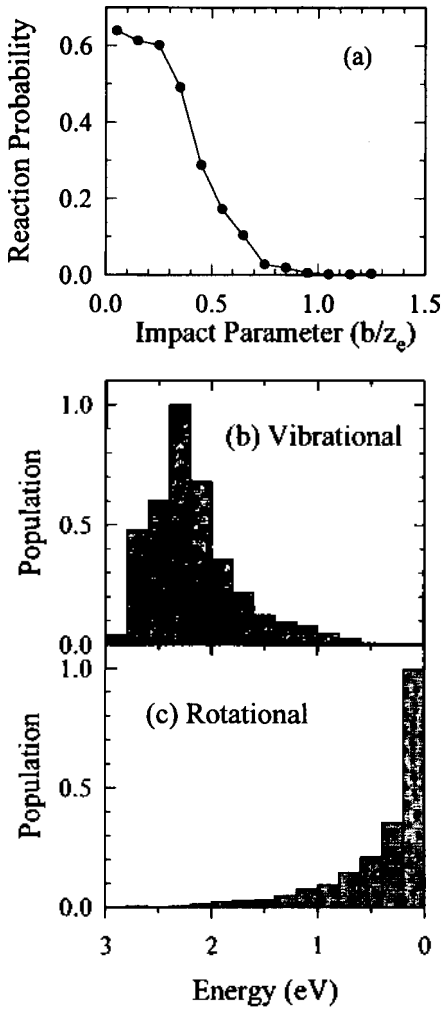

Figure 7. (a) The dependence of the reaction probability on the reduced impact parameter b/z_e. (b) Relative intensity of the vibrational population distribution for H_2. The abscissa is displayed from the right to left to reflect the production of high E_{v,H_2} in small-b collisions. (c) Relative intensity of the rotational population distribution for H_2.

states in calculating reaction probabilities in this system. The weak temperature dependence may also indicate that the principal features of the reaction dynamics discussed above for T_s=0 K remain unchanged.

In Figure 8b, we plotted the total reaction probability over the T_g from 300 to 2500 K with fixed T_s=0 K. This figure shows that the dependence of the P(T) on the gas temperature is also not significant. But, the reaction probability shows a minimum near 1000 K. For analyzing this situation, we calculated the reaction probability P(E) for the fixed value of the collision E in the range of 0.02-0.30 eV, and plotted in Figure 9a. In the former calculation, we also have fixed T_s=0 K. In this figure, it can be noticed that the reaction probability P(E) shows a minimum near E=0.1eV. That is, there is a significant decrease in the probability P(E) when E is raised from 0.02 to 0.10, but beyond this energy range the probability P(E) increases smoothly. On the other hand, the reaction probability P(T) can be calculated by integrating over a Maxwell-Boltzmann distribution of the

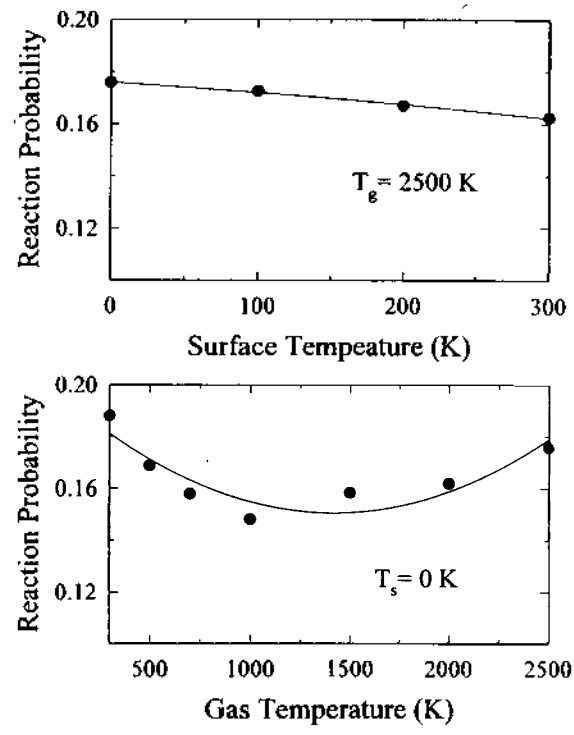

Figure 8. Temperature dependence of reaction probabilities. (a) Dependence on the surface temperature for the fixed T_g of 2500 K and (b) Dependence on the gas temperature for the fixed T_s of 0 K.

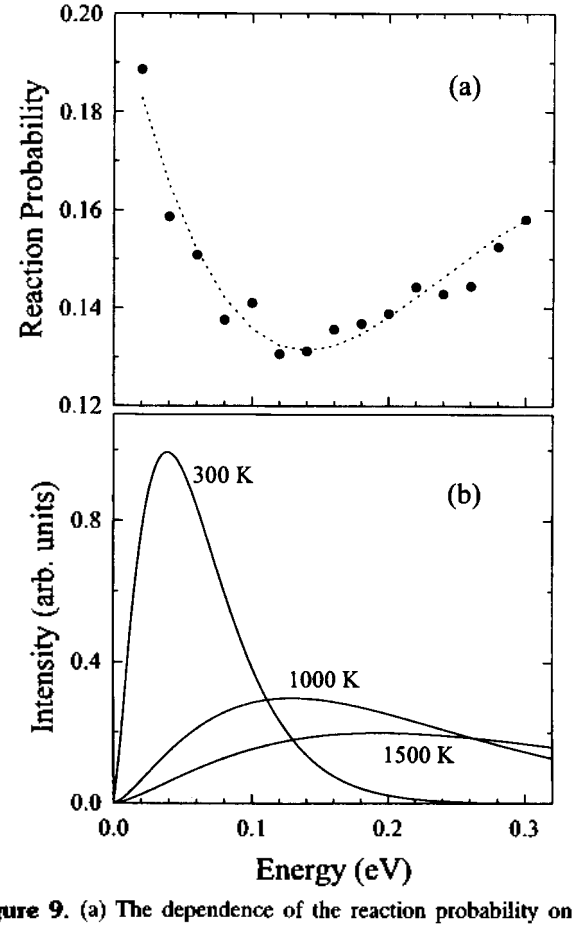

Figure 9. (a) The dependence of the reaction probability on the collision energy. (b) The Maxwell distribution of energies and its dependence on the temperature.

translational energies at a given temperature as $P(T)=\int_0^\infty P(E)\,f(E)\,dE$. We plotted the Maxwell distribution of energies and its dependence on the temperature in Figure 9b. Then, the minimum of the reaction probability near T_g=1000 K can be explained by P(E) and f(E). At the gas temperature 300 K, the maximum intensity of kinetic energy is shown at 0.04 eV, and the reaction probability at this energy is quite large, 0.159. Whereas, at the gas temperature 1000 K, the maximum intensity of kinetic energy is appeared at E=0.13 eV, and the reaction probability shows the minimum, 0.130, in this energy. At T_g=1500 K, the maximum intensity of kinetic energy appears at 0.19 eV, and the reaction probability at this point increase to 0.139. Thus, it can be noticed that the minimum of the reaction probability appears near T_g=1000 K by considering P(E) and f (E).

Concluding Comments

The reaction of H(gas)+H(ads) on an iron surface has been studied by solving the effective equations of motion for the reaction zone atoms and solid-chain atoms. A LEPS potential energy function has been used for the reaction zone interactions, and harmonic representation for the vibrations of solid atoms with the *N*th atom subject to dissipative and stochastic forces. The coupling of the reaction zone motions to seven chain atoms is sufficient to give adequate results for the present gas-surface reaction. Nearly all of the reactive events occur in STP collision, following the ER mechanism. The energy liberated in the reaction is deposited mainly in the vibrational motion of the desorbing H_2. The reaction is treated at various impact parameters b and collision energies. The vibrational energy is largest for the collinear collision and decreases steadily with increasing b. The reaction probability takes also maximum value at b=0. The formation of a large number of highly excited H_2(g) in small-b collisions and a small number of less excited H_2(g) in large-b collisions results in a vibrational population inversion. The probability of H_2 formation is essentially independent of the surface temperature between 0 and 300 K at a given gas temperature. However, the probability of H_2 formation show a minimum near 1000 K when the gas temperature increases from 300 to 2500 K.

Acknowledgment. This research is financially supported by Korea Science and Engineering Foundation.

References

1. Rettner, C. T.; Ashfold, M. N. R. eds. *Dynamics of Gas-Surface Interactions*; Royal Society of Chemistry, Thomas Graham House: Cambridge, England, 1991.
2. Somorjai, G. A. *Intoduction to Surface Chemistry and Catalysis*; Wiley: New York, 1994.
3. Rettner, C. T.; Auerbach, D. J.; Tully, J. C.; Kleyn, A. W. *J. Phys. Chem.* **1996**, *100*, 13021.
4. Laidler, K. J. *Chemical Kinetics*; Harper and Row: New York, 1987, Ch. 7.
5. Tully, J. C. *J. Chem. Phys.* **1980**, *73*, 6333.
6. Thorman, R. P.; Anderson, D.; Bernasek, S. L. *Phys. Rev. Lett.* **1980**, *44*, 743.
7. Kori, M.; Halpern, B. L. *Chem. Phys. Lett.* **1984**, *110*, 223.
8. Hall, R. I.; Cadez, I.; Landau, M.; Pichou, F.; Schermann, C. *Phys. Rev. Lett.* **1988**, *60*, 337.
9. Eenshuistra, P. J.; Bonnie, J. H. M.; Los, J.; Hopman, H. J. *Phys. Rev. Lett.* **1988**, *60*, 341.
10. Schröter, L.; Zacharias, H.; David, R. *Phys. Rev. Lett.* **1989**, *62*, 571.
11. Schermann, C.; Pichou, F.; Landau, M.; Cadez, I.; Hall, R. I. *J. Chem. Phys.* **1994**, *101*, 8152.
12. Rettner, C. T. *Phys. Rev. Lett.* **1992**, *69*, 383.
13. Rettner, C. T.; Auerbach, D. J. *J. Chem. Phys.* **1996**, *104*, 2732.
14. Koleske, D. D.; Gates, S. M.; Schultz, J. A. *J. Chem. Phys.* **1993**, *99*, 5619.
15. Koleske, D. D.; Gates, S. M.; Jackson, B. *J. Chem. Phys.* **1994**, *101*, 3301.
16. Kratzer, P.; Brenig, W. *Surf. Sci.* **1991**, *254*, 275.
17. Jackson, B.; Persson, M. *J. Chem. Phys.* **1992**, *96*, 2378.
18. Jackson, B.; Persson, M. *Surf. Sci.* **1992**, *269/270*, 195.
19. Persson, M.; Jackson, B. *J. Chem. Phys.* **1995**, *102*, 1078.
20. Jackson, B.; Persson, M. *Chem. Phys. Lett.* **1995**, *237*, 468.
21. Shin, H. K. *Chem. Phys. Lett.* **1995**, *244*, 235.
22. Ree, J.; Shin, H. K. *Chem. Phys. Lett.* **1996**, *258*, 239.
23. Nordlander, P.; Holloway, S.; Norskov, J. K. *Surf. Sci.* **1984**, *136*, 59.
24. Christmann, K. *Surf. Sci. Rep.* **1988**, *9*, 1.
25. Adelman, S. A.; Doll, J. D. *J. Chem. Phys.* **1976**, *64*, 2375.
26. Adelman, S. A. *J. Chem. Phys.* **1979**, *71*, 4471.
27. Adelman, S. A. *Adv. Chem. Phys.* **1980**, *44*, 143.
28. Kelly, D.; Verhoef, R. W.; Weinberg, W. H. *J. Chem. Phys.* **1995**, *102*, 3440.
29. Ree, J.; Kim, Y. H.; Shin, H. K. *J. Chem. Phys.* **1996**, *104*, 742.
30. Kubiak, G. D.; Sitz, G. D.; Zare, R. N. *J. Chem. Phys.* **1985**, *83*, 2538.
31. Elkowitz, A. B.; McCreery, J. H.; Wolken, G. Jr. *Chem. Phys.* **1976**, *17*, 423.
32. Huber, K. P.; Herzberg, G. *Constants of Diatomic Molecules*; Van Nostrand Reinhold: New York, 1979; pp 240-253.
33. Cremaschi, P.; Yang, H.; Whitten, J. L. *Surf. Sci.* **1995**, *330*, 255.
34. Huheey, J. E.; Keiter, E. A.; Keiter, R. L. *Inorganic Chemistry: Principles of Structure and Reactivity*, 4th ed.; Harper Collins College Pub.: New York, 1993; p 292.
35. Gray, D. E. Ed. *American Institute of Physics Handbook*; 3rd ed.; McGraw-Hill: New York, 1972; pp 4-116.
36. Nordlander, P.; Holmberg, C.; Harris, J. *Surf. Sci.* **1985**, *152/153*, 702.
37. Vidali, G.; Ihm, G.; Kim, H.-Y.; Cole, M. W. *Surf. Sci. Rep.* **1991**, *12*, 133.
38. Takayanagi, T.; Sato, S. *Chem. Phys. Lett.* **1988**, *144*, 191.
39. Park, S. C.; Nakamura, H.; Ohsaki, A. *J. Chem. Phys.* **1990**, *92*, 6538.
40. Wada, Y.; Takayanagi, T.; Umemoto, H.; Tsunashima, S.; Sato, S. *J. Chem. Phys.* **1991**, *94*, 4896.
41. Kosmas, A. M. *J. Chem. Soc., Faraday Trans.* **1991**, *87*, 517.
42. Urrecha, I.; Serna, I.; Iturbe, J. *Chem. Phys.* **1991**, *154*,

85.
43. *MATH/LIBRARY, IMSL*; Houston: 1989; p 640, 1113.
44. Greenwood, N. N.; Earnshaw, A. *Chemistry of the Elements*; Pergamon Press: Oxford, 1984; p 1248.
45. Gear, C. W. *Numerical initial value problems in ordinary differential equations*; Prentice-Hall: New York, 1971.
46. Peden, C. H. F.; Goodman, D. W.; Weisel, M. D.; Hoffmann, F. M. *Surf. Sci.* **1991**, *253*, 44.
47. Rettner, C. T. *Phys. Rev. Lett.* **1992**, *69*, 383.
48. Kammler, Th.; Lee, J.; Kuppers, J. *J. Chem. Phys.* **1997**, *106*, 7362.
49. See Ref. 1, pp 184-192.

Reactions of Phosphites with Nitroalkene Derivatives: Syntheses of β-Keto Phosphonates and α-Cyanoalkylphosphonates

Dae Young Kim* and Dong Young Oh†

Department of Chemistry, Soonchunhyang University, Asan P.O. Box 97, Chungnam 336-600, Korea
†Department of Chemistry, Korea Advanced Institute of Science and Technology, Taejon 305-701, Korea
Received June 2, 1997

The addition of phosphite derivatives **1** to nitroalkenes **2** afforded α-phosphoryl nitronates which, on treatment MCPBA, were converted β-keto phosphonates **3**. A versatile reaction conditions to generate α-phosphoryl nitronates were examined. α-Cyanoalkylphosphonates **6** were prepared from the diethyl trimethylsilyl phosphite (DTSP) **1c** with nitroalkenes **2** and followed by reduction.

Introduction

Phosphonates are valuable reagents for the construction of carbon-carbon double bonds because their use provides control of olefin regio- and stereoselectivity.[1] β-Keto phosphonates and α-cyanoalkylphosphonates are useful intermediates for homologations of aldehydes and ketones to α, β-unsaturated carbonyl and nitrile compounds *via* the Hornor-Wadsworth-Emmons condensation. Many synthetic approaches for the preparation of β-keto phosphonates have been developed, ranging from the direct Arbuzov reaction of trialkyl phosphites with 1-haloalkyl ketones[2] to the more sophisticated methods using organometallic reagents.[3] They have limitations in terms of the conditions employed, competition from other reactions, and the preparation of starting materials. Recently, β-keto phosphonates were also obtained by either base-induced isomerization of enol phosphates or reaction of ketone enolates with dialkylphosphorochloridite followed by air oxidation.[4] These synthetic methods using n-butyllithium are not convenient in terms of economical cost and safety. Other miscellaneous methods include oxidation of β-hydroxyalkylphosphonates,[5] acylation of 1-(trimethylsilyl)vinylphosphonates,[6] hydrolysis of vinylogous phosphoramides,[7] reaction of 2-(diethoxyphosphinyl)carboxylic acid chlorides with organometallic reagents,[8] the use of (diethoxyphosphoryl)acetonitrile oxides,[9] *via* allenenic intermediates,[10] Pd(0)-catalyzed rearrangement of the 2,3-epoxyalkyl phosphonates,[11] reaction of phosphite with epoxysulfones[12] or chloroepoxide,[13] reaction of silyl enol ethers with phosphite using hypervalent iodine compound,[14] alkylation of β-keto phosphonates,[15] addition of allenicphosphonates with dialkylamines,[16] acylation of triethyl phosphonoacetate[17] or diethyl phosphonoacetic acid.[18] α-Cyanoalkylphosphonates have been obtained by the reaction of triethyl phosphite with 1-bromo-1-nitro-2-phenylethylene[19] and treatment of benzyl cyanide with suitable base and diethyl chlorophosphate.[20]

Our research has focused on the reaction and development of synthetic routes to α-substituted alkylphosphonates,[21] and we have developed the synthetic method from nitroalkene derivatives to β-keto phosphonates[22] and α-cyanoalkylphosphonates.[23] Herein we report the reaction of phosphites with nitroalkene derivatives in more details, providing information on its scopes, mechanisms, and limitations.

Results and Discussion

Synthesis of β-Keto Phosphonates 3. The nitro group is particularly versatile in synthesis since it may be transformed into legion of diverse functionality.[24] It can be readily converted to a carbonyl substituent in the classical Nef reaction.[25] The nitroalkenes are synthetic equivalent of the carbonyl α-cations.[26] Addition of phosphites to nitroalkenes affords α-phosphoryl nitronates in the presence of Lewis acid. These nitronates are converted into β-keto phosphonates under Nef reaction conditions. The addition reaction required one equivalent of Lewis acid and the order of reactivity of Lewis acids was $TiCl_4$>$SnCl_4$>$ZnCl_2$ (Table 1, entries 1-3). Therefore, we performed the addition of triethyl phosphite **1a** with nitroalkenes **2** in the presence of $TiCl_4$ and followed by the Nef reaction with *m*-chloroperbenzoic acid (MCPBA). In general, the Nef reaction often involves either acidic or strongly basic condition. However, the reaction of triethyl phosphite and nitroalkene in the presence of $TiCl_4$ followed by hydrolysis with water gave a β-keto phosphonate with trace amounts. Fortunately,